Measuring the 3D wake of swimming snakes (Natrix tessellata) using volumetric particle image velocimetry

Vincent Stin, Ramiro Godoy-Diana, Xavier Bonnet, Anthony Herrel

© 2023. MANUSCRIPT SUBMITTED TO JOURNAL OF EXPERIMENTAL BIOLOGY (2023) 00, jebxxxxxx. doi:10.1242/jeb.xxxxxx

METHODS & TECHNIQUES

Measuring the 3D wake of swimming snakes (*Natrix tessellata*) using volumetric particle image velocimetry

Vincent Stin[1,2], Ramiro Godoy-Diana[1], Xavier Bonnet[3] and Anthony Herrel[2]

ABSTRACT

We describe a method for measuring the 3D vortical structures produced by an anguilliform swimmer using volumetric velocimetry. The wake of freely swimming dice snakes (*Natrix tessellata*) was quantified, revealing the creation of multiple vortices along the body of the snake due to its undulation. The 3D structure of the vortices generally consisted of paired vortex tubes, some of which were linked together to form a hairpin structure. The observations match predictions from computational fluid dynamic studies of other anguilliform swimmers. Quantitative measurements allowed us to study vortex circulation and size, and global kinetic energy of the flow, which varied with swimming speed, vortex topology, and individual characteristics. Our findings provide a baseline for comparing wake structures of snakes with different morphologies and ecologies and investigating the energetic efficiency of anguilliform swimming.

KEYWORDS: Snake, Swimming, Anguilliform, Hydrodynamics, Volumetric PIV, Vortex

INTRODUCTION

Undulatory swimming kinematics are usually classified in four main modes involving different proportions of the body and/or caudal fin (Lindsey 1978; Sfakiotakis et al. 1999). Among these, anguilliform swimming describes the motion of elongated animals, where the kinematics consist of an undulation that increases in amplitude along the body. Since Lighthill's analytical large amplitude elongated body theory (Lighthill 1971), numerical investigations have been conducted (Kern and Koumoutsakos 2006; Borazjani and Sotiropoulos 2009, 2010; Nangia et al. 2017; Battista 2020a,b; Khalid et al. 2020; Ogunka et al. 2020; Khalid et al. 2021) in order to obtain a estimation of quantities such as forces, pressure fields, and swimming efficiency for an idealized swimmer. Anguilliform swimming hydrodynamics have been experimentally studied on the eels *Anguilla anguilla* (Muller et al. 2001) and *Anguilla rostrata* (Tytell 2004; Tytell and Lauder 2004), the lamprey *Petromyzon marinus* (Gemmell et al. 2016; Du Clos et al. 2019; Lehn 2019), and the catfish *Plotosus lineatus* (Tack et al. 2021), using particle image velocimetry (PIV) in 2D.

[1]PMMH, CNRS, ESPCI Paris-PSL, Sorbonne Université, Université Paris Cité, Paris, France.
[2]UMR7179 MECADEV, Département Adaptation du Vivant, MNHN/CNRS, Paris, France.
[3]Centre d'Étude Biologique de Chizé, CNRS, UMR 7372, Villiers-en-Bois, France.

Authors for correspondence: (vincent.stin@espci.fr)

The elongated and limbless morphology of snakes is associated with over ten different gaits used in various environments (Jayne 2020), with swimming kinematics first studied quantitatively by Taylor (1952) inspired by the work of Gray (1933). Snakes' great diversity in size and shape makes them ideal to study anguilliform locomotion, and their numerous independent radiations into aquatic environments provide insight into the adaptation of elongated limbless tetrapods to this environment. However, apart from prey capture studies (Van Wassenbergh et al. 2010; Segall et al. 2019), a hydrodynamic analysis based on live swimming snake data has yet to be attempted.

Although 2D PIV helps to understand aquatic locomotion dynamics, 3D velocimetry is necessary to fully describe the vortex dynamics produced by a moving finite body (Tytell et al. 2008), especially in out-of-plane movements as in swimming snakes. The main methods are synthetic aperture PIV (e.g., Lehn 2019; Mendelson and Techet 2020), tomographic PIV (Skipper et al. 2019), and digital defocusing PTV (e.g., Flammang et al. 2011; Bartol et al. 2016). These methods instantly capture the entire 3D unsteady flow field, but flow field measurements of swimming animals are scarce. Aside from unpublished work on lampreys (Lehn 2019), the 3D wake of an anguilliform swimmer has not been characterized experimentally.

We propose a method to examine the 3D flow induced by an anguilliform swimmer using a free-swimming dice snake (*Natrix tessellata*) as our model. Using DDPTV, we measured the wake and investigated the vortical structure. We compared results to previous computational fluid dynamics and 2D experimental PIV studies.

MATERIAL AND METHODS

Animals and swimming behaviour

Swimming kinematics and PIV data were obtained from three (one male and two females) adult captive dice snakes (*Natrix tessellata*). Dice snakes are semi-aquatic snakes and were chosen for their relatively small size.

A first set of trials was made to characterize the swimming kinematics of *Natrix tessellata* as no data are available in the literature and because the kinematic parameters of swimming snakes are generally scarce. The snakes were freely swimming in a plexiglass tank (length = 400 cm, width = 40 cm, height = 30 cm, water height = 22 cm). Animals were filmed in ventral view (Phantom MIRO, 1000 fps). Kinematic parameters were extracted by digitizing the snake's midline using an custom-written MATLAB routine. We measured the following anatomical and kinematic parameters: the total length, from the tip of the snout to the tip of the tail (L), maximal body diameter (D), body mass (m), forward swimming speed (U), tailbeat frequency (f), peak-to-peak amplitude of the tail (A),

Journal of Experimental Biology (2023) 00, jebxxxxxx. doi:10.1242/jeb.xxxxxx

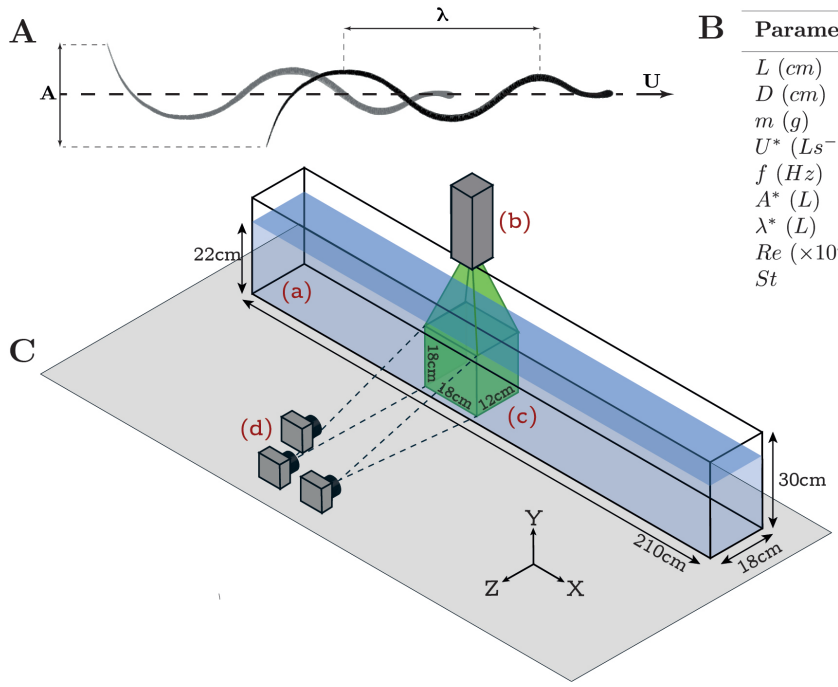

Parameter	Natrix M	Natrix F1	Natrix F2
L (cm)	64.7	83.4	82.4
D (cm)	1.06	1.63	1.56
m (g)	58	142	119
U^* (Ls^{-1})	0.60 ± 0.14	0.53 ± 0.1	0.40 ± 0.06
f (Hz)	1.78 ± 0.34	2.15 ± 0.42	1.67 ± 0.29
A^* (L)	0.15 ± 0.018	0.11 ± 0.023	0.10 ± 0.015
λ^* (L)	0.43 ± 0.037	0.40 ± 0.050	0.38 ± 0.039
Re $(\times 10^3)$	4.53 ± 1.07	8.07 ± 1.51	5.67 ± 0.91
St	0.45 ± 0.045	0.46 ± 0.061	0.44 ± 0.056

Fig. 1. Experimental setup and snake kinematics. (A) Superimposed images of a snake at two consecutive maxima of tail deflection. The peak-to-peak amplitude A, tailbeat frequency f and the forward velocity U are measured by finding the peaks in the lateral excursion of the tail-tip over time for at least one full tailbeat cycle. The body wave length λ is measured when two adjacent crests are clearly visible on the snake body. (B) Anatomical & kinematic parameters gathered during the swimming behaviour experiment with the asterisk meaning that the parameter was divided by the snake length. Number of swimming trials: $N_M = 17$, $N_{F1} = 11$, $N_{F2} = 11$. Results are presented as means±s.d. (C) Volumetric imaging setup. a: Water tank, b: Nd:YAG laser (Quantel Evergreen), c: Measurement volume, d: Camera frame. (D) Boxplot of mean voluntary forward velocity of the swimming snakes during the PIV swimming trials ($N_M = 31$, $N_{F1} = 52$, $N_{F2} = 29$).

and the body wavelength (λ). The Reynolds and Strouhal numbers were also computed as:

$$Re = \frac{UD}{\nu} \tag{1}$$

$$St = \frac{fA}{U} \tag{2}$$

where ν is the water kinematic viscosity. The general swimming kinematic parameters are summarized in Fig.1.B and permit a broad estimation of the swimming behaviour of the test animals under laboratory conditions. Although conducted separately from the PIV experiments, these trials have the potential to be performed concurrently in a separate study, with appropriate laser filtering in place. An example of a swimming trial video is accessible in the supplementary materials.

Experimental PIV setup

In order to quantify the flow around a swimming snake we used a volumetric three-component DDPTV setup (V3V-9000-CS system, TSI ; Fig.1.C). The experiments were conducted in a water-filled plexiglass tank (length = 210 cm, width = 18 cm, height = 30 cm, water height = 22 cm). A narrower tank was chosen in order to increase the chances of the snake to swim through the measurement volume without over-constraining the kinematics. The water was seeded with 50 μm polyamide particles (PSP-50, Dantec Dynamics) with a concentration of around 5×10^{-2} ppp (Cambonie and Aider 2014). The tank was illuminated from above by a 14 Hz pulsed 200 mJ dual head Nd:YAG laser (Quantel Evergreen) expanded with two -25 mm cylindrical lenses. The particles were filmed by three CCD arrays (Powerview Plus 4MP-HS) with 50 mm camera lenses (Nikon AF Nikkor, aperture f/16) mounted on a 170 mm equilateral triangular frame (V3V 9000-CS). The acquisition setup was piloted by the INSIGHT V3V-4G software and calibrated as explained by Troolin and Longmire (2010). The resulting measurement volume is the intersection between the fields of view of the cameras and the laser cone. Its dimension is approximately $18 \times 18 \times 12$ cm and it is centered on the water tank in width (Z-axis) and height (Y-axis).

Recording procedure

During each trial the snake was placed at one side of the tank and allowed to swim. When put into the water snakes typically swam to the other side of the tank along the X direction, passing through the measurement volume while being recorded by the cameras at a frequency of 14 Hz. Preliminary trials were conducted to estimate the best ΔT between two consecutive PIV frames so that displacement of the seeding particles does not exceeded six pixels. The resulting ΔT ranged between 1 ms and 2.5 ms. As the width of the measurement volume was smaller than the width of the water tank, only the trials were the snake entirely swam through it were retained. The PIV swimming trials were performed on six different days over the course of several weeks. During the first two recording days, females were gravid which impacted their body mass and diameter. The measurements in Table 1 were made after the eggs were laid. A total of 112 sequences of free swimming *Natrix tessellata* with at least one tailbeat in the measurement volume were

recorded. The number of sequences were respectively 31, 52 and 29 for *Natrix* M, *Natrix* F1 and *Natrix* F2.

Data processing

Image masking

In order to avoid artefacts induced by the presence of the snake's body on the raw images during the PIV analysis, the snake was removed from the images with the help of a custom-written masking routine in MATLAB using the Image Processing Toolbox.

PIV Processing

The images were then processed using the INSIGHT V3V-4G software in order to obtain the vector fields. The main steps of the data processing are: (1) 2D particle identification in the images of each camera using a Gaussian fitting (Levenberg–Marquardt algorithm). (2) 3D particle identification, the correspondence of a particle in one image to the same particle in the other two images is carried in agreement with the calibration. The fine search tolerance is set to 0.5 px and the coarse search tolerance to 1 px. (3) The velocity is processed using the 3D displacement between two consecutive frames with a relaxation algorithm (Pereira et al. 2006). (4) The neighbor tracking reconstruction algorithm uses the trajectories from the neighboring particles to find the probable location of a missing triplet at time $t + \Delta$T. (5) The randomly spaced vectors are finally interpolated using a Gaussian-weighted algorithm (Pereira and Gharib 2002), resulting in a $74 \times 74 \times 43$ evenly spaced vector grid with a 2.5 mm resolution.

Base change

Vector fields were processed using code written in MATLAB. The swimming trials being in free swimming conditions, the movements of the snake in the measurement volume can be quite different from one sequence to another, which makes the comparison challenging. In order to tackle this problem, we changed the regular Cartesian coordinate system (XYZ) to a new rotated coordinate system ($X_{rot}YZ_{rot}$) for each swimming trial. For each recorded sequence the water jet created by the last tailbeat was tracked with a velocity thresholding method. The trajectory of the jet was estimated by a linear regression of the superimposed position of the jet center. A new base was then created by a rotation around the Y-axis so that the new X_{rot} axis was co-linear to the jet's trajectory and the Z_{rot} axis perpendicular to it.

Hydrodynamic parameters

The flow field induced by the swimming snake was monitored from its detection in the volume until it either reached the edges of the working volume or dissipated. The unsteadiness was quantified by computing the Q-criterion of the vector field. Q is defined as the second invariant of the velocity gradient tensor (Hunt et al. 1988; Jeong and Hussain 1995):

$$Q = \frac{1}{2}(\| \Omega \|^2 - \| S \|^2) \tag{3}$$

where Ω is the antisymmetric part and S the symmetric part of the tensor. The positive values of Q indicate the parts of the flow field where vorticity dominates over the viscous stress. The strength of the vortices was estimated by computing the circulation of the vortex cores:

$$\Gamma = \oint_C \vec{v} \cdot d\vec{l} = \int_S \vec{\omega} \cdot \vec{n} dS \tag{4}$$

where ω is the vorticity vector and n the normal vector. The surfaces S of the vortex cores are identified by using the Γ_2 criterion (Graftieaux et al. 2001) in the rotated $X_{rot}Y$ planes co-linear to the jet trajectory so that a vortex core is always present in the planes. The vortex size d is defined by the distance between the center of the positive and negative vortex cores:

$$d = \sqrt{(x_+ - x_-)^2 + (y_+ - y_-)^2} \tag{5}$$

where (x_+, y_+) and (x_-, y_-) are the coordinates of the centers of the positive and negatives vortex cores in the $X_{rot}Y$ planes. In order to compare the results between the different individuals and sequences, the hydrodynamic parameters are non-dimensionalized by the mean forward swimming speed U of the snake during the measurement period and the snake diameter D :

$$\Gamma^* = \frac{\Gamma}{UD} \tag{6}$$

$$d^* = \frac{d}{D} \tag{7}$$

The kinetic energy of the wake in the whole measurement volume is defined as :

$$E = \frac{\rho}{2} \int_V \| u \|^2 \, dV \tag{8}$$

where ρ is the water density, V the measurement volume and $\| u \|$ the velocity magnitude. To quantify differences in the hydrodynamic parameters across individual sequences we focused on trials where at least one tail beat vortex was clearly visible and where measurements were possible ($N_M = 12$; $N_{F1} = 13$; $N_{F2} = 14$).

RESULTS & DISCUSSION

Vortex characterisation

Although the snakes swam with the characteristic lateral undulation of an anguilliform swimmer in the frontal plane (XZ), there were also noticeable, albeit smaller, oscillations in the sagittal plane (XY). The tail was often positioned below the body and the tailbeats were downward facing. The mean swimming speed in body lengths per second across the swimming trials was, respectively, $U_M = 0.51\ Ls^{-1}$, $U_{F1} = 0.37\ Ls^{-1}$ and $U_{F2} = 0.34\ Ls^{-1}$ (Fig.1.D).

During a typical swimming sequence, vortices were shed after each change of direction of the swimmer's body during oscillatory movements. The displacement of the body created two vortex tubes of opposite rotation (Fig.2.A,B) on its top and bottom, which in some cases became connected. The shed vortices were tilted at an angle of approximately 30° to 40° to the swimming direction (Fig.2.C). Their trajectory was mostly linear with a tendency to curl. Body vortices with similar topologies and dynamics were also observed.

Journal of Experimental Biology (2023) 00, jebxxxxxx. doi:10.1242/jeb.xxxxxx

The circulation of the vortex cores rapidly increased in magnitude just after the tail beat and reached a maximum before decreasing (Fig.2.D). The positive and the negative vortex cores displayed symmetrical variations during the observed time period. During its lifetime, the vortex size gradually increased (Fig.2.E) and changed from a flattened into a more circular shape. The kinetic energy of the wake increased starting from the moment when the swimmer enters the measurement volume. After the final tailbeat of the swimmer, the perturbations dissipate and the kinetic energy decreases (Fig.2.F).

Comparison of parameters

Across the swimming sequences, the dimensional maximal circulation ranged from around 18 to 51 cm^2s^{-1}, 25 to 70 cm^2s^{-1} and 22 to 88 cm^2s^{-1} for *Natrix* M, *Natrix* F1, and *Natrix* F2, respectively. The non-dimensional circulation Γ^* ranged approximately between 0.5 and 1.5. The maximum vortex size was between approximately 2.5 and 5.3 cm, 2.7 and 5.2 cm, and 2.6 and 5.4 cm for *Natrix* M, *Natrix* F1, and *Natrix* F2 respectively. A Spearman correlation (R=0.8, P<0.05) showed that there was an increasing monotonic trend between the maximal vortex size and the maximal circulation. As the maximal circulation is usually measured

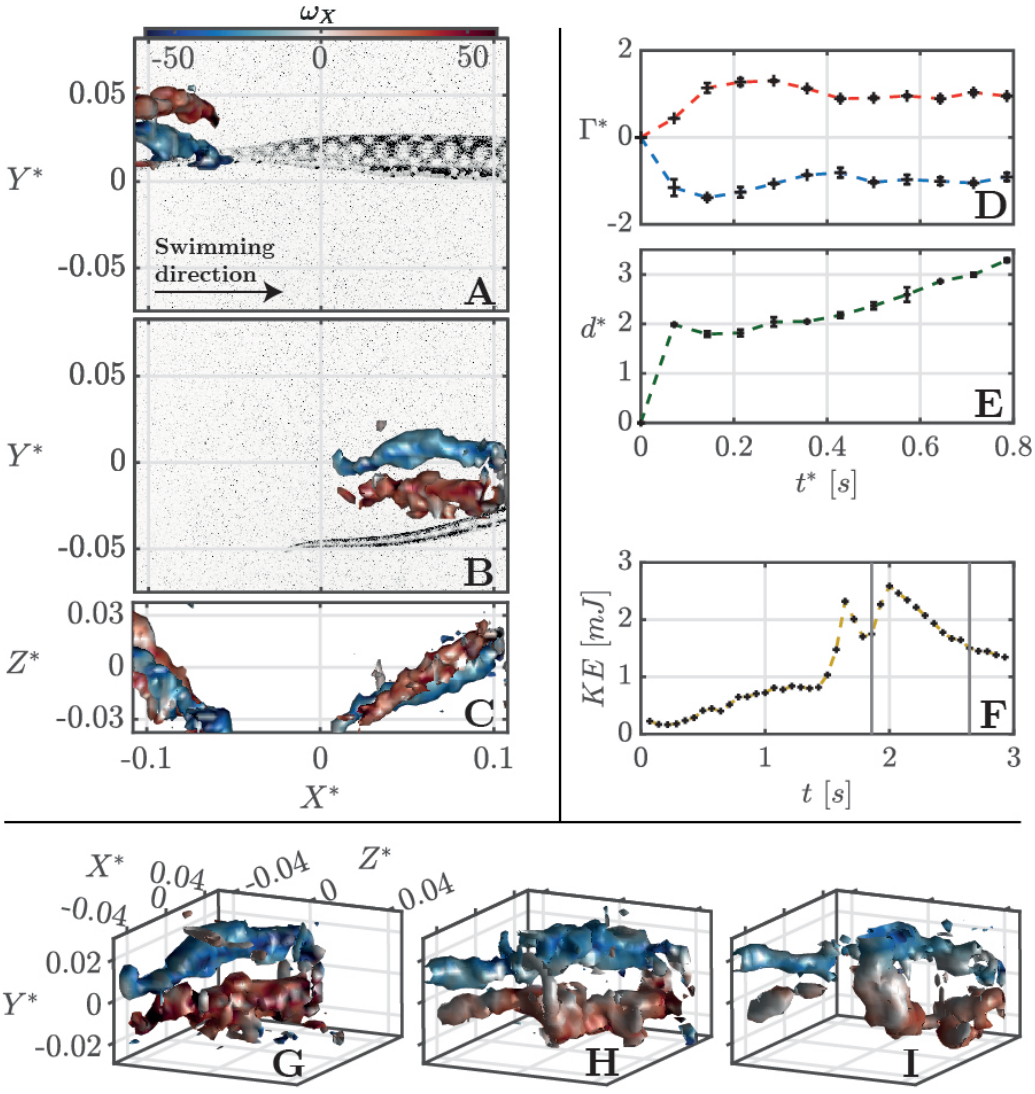

Fig. 2. Results. (A,B,C) Trailing edge vortices in the measurement volume during a swimming trial highlighted with Q-criterion isosurfaces (Q = 80) colored by ω_x. (A,B) Side view of two consecutive trailing edge vortices ($\Delta T = 286\ ms$, half of a tailbeat cycle) with the corresponding snake image (*Natrix* F1) captured by the PIV cameras. (C) Top view of the superimposed isosurfaces shown on (A) and (B) at their respective times showcasing the angle between two consecutive vortices. (D,E,F) Measured hydrodynamic parameters during the swimming trial. (D) Positive (red) and negative (blue) vortex core non-dimensionalized circulation of the trailing edge vortex (B) from the frame before its detection ($t^* = 0$) to the time when it reaches the edge of the measurement volume. (E) Size-adjusted vortex size evolution. Values are the mean values in three consecutive planes centered on the vortex path. Error bars are s.d. (F) Evolution of the kinetic energy in the whole measurement volume during the swimming trial. The two vertical lines correspond to the beginning and the end of t^*. (G,H,I) 3D view showcasing the main steps of the behaviour of a hairpin-like vortex with the example of the trailing edge vortex in (B). (G) Two vortex tubes of opposite rotation ($t^* = 71\ ms$). (H) Bridging of the two vortex tubes ($t^* = 285\ ms$). (I) Separation of the tubes before the bridge and the shape of the structure is getting rounder ($t^* = 500\ ms$). The mean vorticity at the bridge section ($\omega_Y = 15.08\ s^{-1}$) is similar to the vorticity of the vortex tubes ($\omega_X = 15.45\ s^{-1}$). The corresponding video can be accessed in the supplementary materials.

near the beginning of the vortex lifetime, this means that a high initial circulation is likely to yield a bigger vortex.

A Spearman correlation (R=0.7, P<0.05) between the maximal kinetic energy in the whole measurement volume during the entire swimming sequence and the maximal circulation of the tailbeat vortex showed an increasing monotonic trend. This means that there is a tight scaling between the local hydrodynamic parameters of the vortices (i.e., the circulation) and the global parameters (i.e., the kinetic energy of the fluid in the whole measurement field).

Discussion

As the wake is the footprint of a swimmer, it is crucial to fully capture it in order to maximise the understanding of the fluid-structure interactions between the body and the water. The 2D PIV experiments on eels by Muller et al. (2001) in the frontal plane have led to the prediction that the 3D vortical structure of an anguilliform swimmer should resemble a vortex ring. Tytell and Lauder (2004) were skeptical about the true roundness of the vortex and the computational work of Borazjani and Sotiropoulos (2009) suggested that the wakes were in fact vortex loops stretched in the streamwise direction or "hairpin-like" vortices. The traditional plane to measure the swimmer's wake in the existing literature is the frontal plane (XZ) without looking at the other ones (Fig.3.A,B,C). Our experimental results in the frontal plane are in accordance with the 2D vortex behaviour in the existing anguilliform swimming studies (Fig.3.D) with the creation of two counter-rotating vortex cores during a tailbeat cycle. The 3D velocimetry method presented here reveals that these vortex cores observable in the frontal plane are the links between the vortex tubes stretched in the swimming direction (Fig.3.E). These links are created after each change of direction of the tail.

The observed three-dimensional vortex topologies were either hairpin-like, tubular or turbulent without any clear cohesion. We observed hairpin-like and tubular structures in most of the analysed swimming sequences. A lack of cohesion was observed essentially only when the snake kinematics involved strongly out-of-plane motions, changes of direction, or acceleration/deceleration sequences. These different vortex topologies have been predicted by CFD studies (Kern and Koumoutsakos 2006; Borazjani and Sotiropoulos 2009; Khalid et al. 2021), and associated to different kinematic parameters such as the tailbeat amplitude, frequency, and body wavelength.

As the DDPTV enables the observation of the full wake structure, our measurements revealed the different stages of the formation of the hairpin vortices. The shedding of two vortex tubes of opposite rotation immediately after a tailbeat (Fig.2.G) creates a bridge

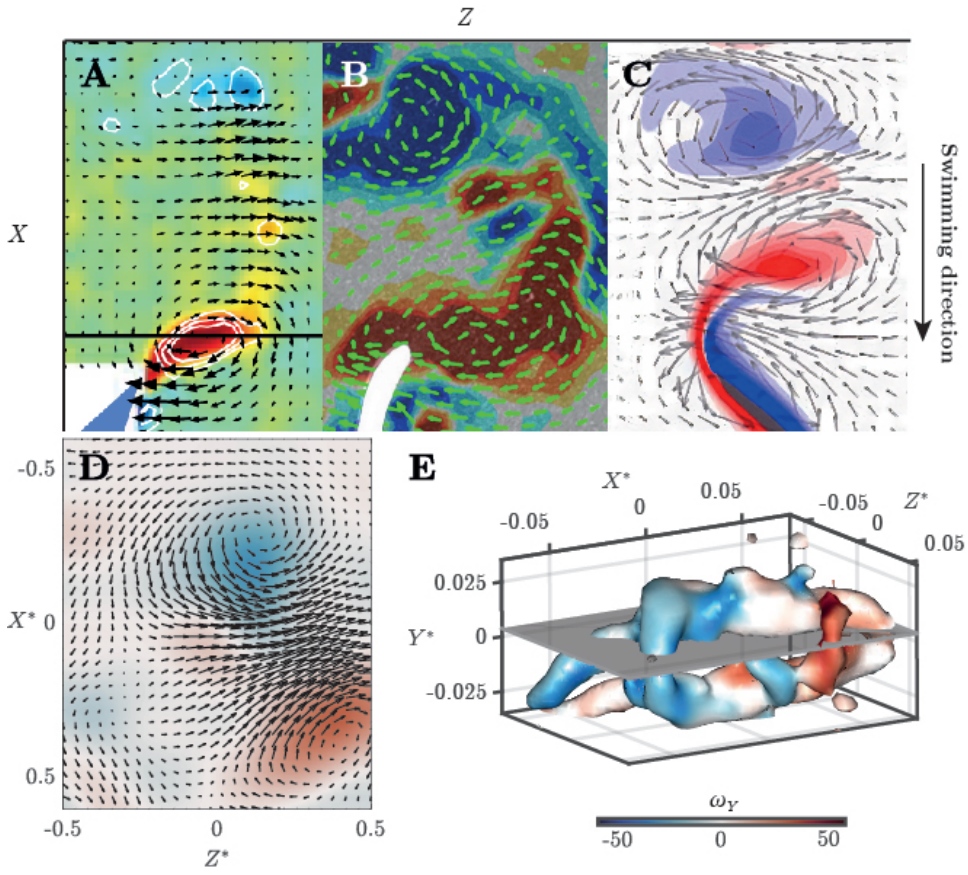

Fig. 3. Vortex comparison. (A,B,C,D) Trailing edge vortices in the frontal plane (XZ) from different studies. The swimmers are swimming along the X axis and the visible vortex cores are the result of a full tailbeat cycle. Vector fields from (A) an eel (Tytell and Lauder 2004) (B) a lamprey (Gemmell et al. 2016) (C) an anguilliform swimmer CFD model (Kern and Koumoutsakos 2006) and (D) our results. The flow field in (D) is smoothed with a 3D Gaussian filter ($\sigma = 1.25$) to enhance the illustration of the dipolar vortex structure only (note that the quantitative computations of vortex circulation and kinetic energy were performed on the unfiltered velocimetry output). The corresponding ω_Y-colored 3D plot (E) suggests that the vortex structure is more complex than it appears in a 2D plane. The grey plane is the location of the velocity field (D).

where the vortex tubes interact (Fig.2.H), leading to their connection and detachment before the bridge (Fig.2.I). These steps are similar to events in coherent packets of hairpin vortices in channel flow (Zhou et al. 1999). The rounding of the vortex structure after the bridging step is also reminiscent of the Ω-shaped vortex created by self-induction of the hairpin vortex. Despite the relatively slow frame rate, our 3D measurement allowed us to observe the bridging step.

The shedding of vortices was also witnessed more anteriorly on the body. The production of body vortices has been described by Gemmell et al. (2016) for lampreys where a particular attention was given to the bending of the body. In addition to transverse motion, the body has an angular velocity in the transverse plane (YZ). The body surface rotation helps to rotate the fluid and eases the shedding of adjacent vortices. The production of counter-rotating vortex tubes along the body has been suggested to generate additional thrust (Fu and Liu 2015) during swimming. In the case of gliding snakes, a CFD study showed that the body-induced vortices produced lift along the body (Gong et al. 2022). The body vortices may therefore have a double function of propelling and stabilising the swimmer.

The maximal circulation measured for the three swimmers was similar to the ones measured in smaller anguilliform swimmers: $\sim 20\ cm$ eels (Tytell and Lauder 2004) and $\sim 10\ cm$ lampreys (Gemmell et al. 2016). The circulation of small hairpin vortices decreases exponentially after attaining a maximum because of the viscous interactions of the counter-rotating vortex tubes (Sabatino and Maharjan 2015). On the other hand, the circulation of laminar vortex rings slowly decreases after the maximum (Rosenfeld et al. 1998). In our results, depending on the swimming trial, the circulation either decreases or stays relatively constant. The decreasing vortex circulation is probably due to the viscous interactions with either the counter rotating vortex tubes or surrounding vortices created by the other tail beats. The relatively constant or slowly decreasing circulation, on the other hand, behaves like a laminar vortex ring.

Studies on vortex rings show that the diameter of the vortex rapidly increases, attains a maximum, and then asymptotically decreases to a constant value (Arakeri et al. 2004). The distance between the vortex cores observed here follows the same pattern as they either increase or stay relatively constant. This means that the vortices with an increasing distance are in the first part of their lifetime and the ones with a relatively constant distance are likely to be near the end of their lifetime. Our data further suggests a relationship between the circulation and vortex size.

As the experiments were done in a still-water tank, the displacement of the water was essentially caused by the swimming snakes. The kinetic energy of the water measured is therefore the energy that was transferred by the snake minus the dissipation. Computational studies found faster swimming kinematics result in stronger vortices (Kern and Koumoutsakos 2006; Bhalla et al. 2013). Gravid snakes had larger body diameter and higher mass but proportionally less locomotor muscle due to eggs which may impact locomotor performance (Seigel et al. 1987). Gravid snakes shed vortices with high circulation and size, producing the highest overall kinetic energy, suggesting they adjust swimming effort at a higher cost. Complementary results from other species may provide an explanation for the observed phenomenon of gravid snakes exhibiting less swimming activity compared to non-gravid individuals (Aubret et al. 2005).

Volumetric measurements of the wake can be used as tools for non-invasive estimations of the swimming performance (Li and Mendelson 2023). Coupled with 3D kinematic data, the results of this method could be used for interspecific comparisons of the swimming performance of snakes. This would lead to a better understanding of the differences of swimming efficiency in snakes with different lifestyles, shapes, and ecologies.

Competing interests

The authors declare no competing or financial interests.

Acknowledgements

This research was supported by ANR DRAGON2 (ANR-20-CE02-0010). We thank Jake Socha and an anonymous reviewer for helpful and constructive comments on an earlier version of the manuscript.

Contribution

A.H., X.B. and R.G.D. conceived the study; V.S. carried out experimental work; V.S. carried out data analysis; V.S. wrote the manuscript; A.H., X.B. and R.G.D. revised the manuscript. All authors gave final approval for publication.

Data availability

All data and codes are available from the authors upon request.

References

Arakeri, J., Das, D., Krothapalli, A., and Lourenco, L. (2004). "Vortex ring formation at the open end of a shock tube: a particle image velocimetry study". In: *Phys. Fluids* 16.4, pp. 1008–1019.

Aubret, F., Bonnet, X., Shine, R., and Maumelat, S. (2005). "Swimming and pregnancy in Tiger snakes, *Notechis scutatus*". In: *Amphib.-reptil.* 26.3, pp. 396–400.

Bartol, I. K., Krueger, P. S., Jastrebsky, R. A., Williams, S., and Thompson, J. T. (2016). "Volumetric flow imaging reveals the importance of vortex ring formation in squid swimming tail-first and arms-first". In: *J. Exp. Biol.* 219.3, pp. 392–403.

Battista, N. A. (2020a). "Diving into a simple anguilliform swimmer's sensitivity". In: *Integr. Comp. Biol.* 60.5, pp. 1236–1250.

Battista, N. A. (2020b). "Swimming through parameter subspaces of a simple anguilliform swimmer". In: *Integr. Comp. Biol.* 60.5, pp. 1221–1235.

Bhalla, A. P. S., Griffith, B. E., and Patankar, N. A. (2013). "A Forced Damped Oscillation Framework for Undulatory Swimming Provides New Insights into How Propulsion Arises in Active and Passive Swimming". In: *PLoS Comput. Biol.* 9.6, e1003097.

Borazjani, I. and Sotiropoulos, F. (2009). "Numerical investigation of the hydrodynamics of anguilliform swimming in the transitional and inertial flow regimes". In: *J. Exp. Biol.* 212.4, pp. 576–592.

Borazjani, I. and Sotiropoulos, F. (2010). "On the role of form and kinematics on the hydrodynamics of self-propelled body/caudal fin swimming". In: *J. Exp. Biol.* 213.1, pp. 89–107.

Cambonie, T. and Aider, J.-L. (2014). "Seeding optimization for instantaneous volumetric velocimetry. Application to a jet in crossflow". In: *Opt. Lasers Eng.* 56, pp. 99–112.

Du Clos, K. T., Dabiri, J. O., Costello, J. H., Colin, S. P., Morgan, J. R., Fogerson, S. M., and Gemmell, B. J. (2019). "Thrust generation during steady swimming and acceleration from rest in anguilliform swimmers". In: *J. Exp. Biol.* 222.22, jeb212464.

Flammang, B. E., Lauder, G. V., Troolin, D. R., and Strand, T. E. (2011). "Volumetric imaging of fish locomotion". In: *Biol. Lett.* 7.5, pp. 695–698.

Fu, Z. and Liu, H. (2015). "Transient force augmentation due to counter-rotating vortex ring pairs". In: *J. Fluid Mech.* 785, pp. 324–348.

Gemmell, B. J., Fogerson, S. M., Costello, J. H., Morgan, J. R., Dabiri, J. O., and Colin, S. P. (2016). "How the bending kinematics of swimming lampreys build negative pressure fields for suction thrust". In: *J. Exp. Biol.* 219.24, pp. 3884–3895.

Gong, Y., Wang, J., Zhang, W., Socha, J. J., and Dong, H. (2022). "Computational analysis of vortex dynamics and aerodynamic performance in flying-snake-like gliding flight with horizontal undulation". In: *Phys. Fluids* 34.12, p. 121907.

Graftieaux, L., Michard, M., and Grosjean, N. (2001). "Combining PIV, POD and vortex identification algorithms for the study of unsteady turbulent swirling flows". In: *Meas. Sci. Technol.* 12.9, p. 1422.

Gray, J. (1933). "Studies in animal locomotion: I. The movement of fish with special reference to the eel". In: *J. Exp. Biol.* 10.1, pp. 88–104.

Hunt, J. C., Wray, A. A., and Moin, P. (1988). "Eddies, streams, and convergence zones in turbulent flows". In: *Studying turbulence using numerical simulation databases, 2. Proceedings of the 1988 summer program*, pp. 193–208.

Jayne, B. C. (2020). "What defines different modes of snake locomotion?" In: *Integr. Comp. Biol.* 60.1, pp. 156–170.

Jeong, J. and Hussain, F. (1995). "On the identification of a vortex". In: *J. Fluid Mech.* 285, pp. 69–94.

Kern, S. and Koumoutsakos, P. (2006). "Simulations of optimized anguilliform swimming". In: *J. Exp. Biol.* 209.24, pp. 4841–4857.

Khalid, M. S. U., Wang, J., Akhtar, I., Dong, H., Liu, M., and Hemmati, A. (2021). "Why do anguilliform swimmers perform undulation with wavelengths shorter than their bodylengths?" In: *Phys. Fluids* 33.3, p. 031911.

Khalid, M. S. U., Wang, J., Dong, H., and Liu, M. (2020). "Flow transitions and mapping for undulating swimmers". In: *Phys. Rev. Fluids.* 5.6, p. 063104.

Lehn, A. M. (2019). "Volumetric analysis of lamprey hydrodynamics using synthetic aperture particle image velocimetry". PhD thesis. Massachusetts Institute of Technology.

Li, D. J. and Mendelson, L. (2023). "Volumetric measurements of wake impulse and kinetic energy for evaluating swimming performance". In: *Exp. Fluids* 64.3, p. 47.

Lighthill, M. J. (1971). "Large-amplitude elongated-body theory of fish locomotion". In: *Proc. R. Soc. London, Ser. B* 179.1055, pp. 125–138.

Lindsey, C. (1978). "Form, function and locomotory habits in fish". In: *Locomotion*.

Mendelson, L. and Techet, A. H. (2020). "Jumping archer fish exhibit multiple modes of fin–fin interaction". In: *Bioinspir. Biomim.* 16.1, p. 016006.

Muller, U. K., Smit, J., Stamhuis, E. J., and Videler, J. J. (2001). "How the body contributes to the wake in undulatory fish swimming: flow fields of a swimming eel (*Anguilla anguilla*)". In: *J. Exp. Biol.* 204.16, pp. 2751–2762.

Nangia, N., Bale, R., Chen, N., Hanna, Y., and Patankar, N. A. (2017). "Optimal specific wavelength for maximum thrust production in undulatory propulsion". In: *PLoS ONE* 12.6, e0179727.

Ogunka, U. E., Daghooghi, M., Akbarzadeh, A. M., and Borazjani, I. (2020). "The ground effect in anguilliform swimming". In: *Biomimetics* 5.1, p. 9.

Pereira, F. and Gharib, M. (2002). "Defocusing digital particle image velocimetry and the three-dimensional characterization of two-phase flows". In: *Meas. Sci. Technol.* 13.5, pp. 683–694.

Pereira, F., Stüer, H., Graff, E. C., and Gharib, M. (2006). "Two-frame 3D particle tracking". In: *Meas. Sci. Technol.* 17.7, pp. 1680–1692.

Rosenfeld, M., Rambod, E., and Gharib, M. (1998). "Circulation and formation number of laminar vortex rings". In: *J. Fluid Mech.* 376, pp. 297–318.

Sabatino, D. R. and Maharjan, R. (2015). "Characterizing the formation and regeneration of hairpin vortices in a laminar boundary layer". In: *Phys. Fluids* 27.12, p. 124104.

Segall, M., Herrel, A., and Godoy-Diana, R. (2019). "Hydrodynamics of frontal striking in aquatic snakes: drag, added mass, and the possible consequences for prey capture success". In: *Bioinspir. Biomim.* 14.3, p. 036005.

Seigel, R. A., Huggins, M., and Ford, N. B. (1987). "Reduction in locomotor ability as a cost of reproduction in gravid snakes". In: *Oecologia* 73.4, pp. 481–485.

Sfakiotakis, M., Lane, D. M., and Davies, J. B. C. (1999). "Review of fish swimming modes for aquatic locomotion". In: *IEEE J. Ocean. Eng.* 24.2, pp. 237–252.

Skipper, A., Murphy, D., and Webster, D. (2019). "Characterization of hop-and-sink daphniid locomotion". In: *J. Plankton Res.* 41.2, pp. 142–153.

Tack, N. B., Du Clos, K. T., and Gemmell, B. J. (2021). "Anguilliform Locomotion across a Natural Range of Swimming Speeds". In: *Fluids* 6.3, p. 127.

Taylor, G. I. (1952). "Analysis of the swimming of long and narrow animals". In: *Proc. R. Soc. London, Ser. A* 214.1117, pp. 158–183.

Troolin, D. R. and Longmire, E. K. (2010). "Volumetric velocity measurements of vortex rings from inclined exits". In: *Exp. Fluids* 48.3, pp. 409–420.

Tytell, E. D. (2004). "The hydrodynamics of eel swimming II. Effect of swimming speed". In: *J. Exp. Biol.* 207.19, pp. 3265–3279.

Tytell, E. D. and Lauder, G. V. (2004). "The hydrodynamics of eel swimming: I. Wake structure". In: *J. Exp. Biol.* 207.11, pp. 1825–1841.

Tytell, E. D., Standen, E. M., and Lauder, G. V. (2008). "Escaping Flatland: Three-Dimensional Kinematics and Hydrodynamics of Median Fins in Fishes". In: *J. Exp. Biol.* 211.2, pp. 187–195.

Van Wassenbergh, S., Brecko, J., Aerts, P., Stouten, I., Vanheusden, G., Camps, A., Van Damme, R., and Herrel, A. (2010). "Hydrodynamic constraints on prey-capture performance in forward-striking snakes". In: *J. R. Soc. Interface* 7.46, pp. 773–785.

Zhou, J., Adrian, R. J., Balachandar, S., and Kendall, T. (1999). "Mechanisms for generating coherent packets of hairpin vortices in channel flow". In: *J. Fluid Mech.* 387, pp. 353–396.